Characterization of a New Fully Recycled Carbon Fiber Reinforced Composite Subjected to High Strain Rate Tension

H. Meftah [1,2] · **S. Tamboura** [1] · **J. Fitoussi** [2] · **H. BenDaly** [1] · **A. Tcharkhtchi** [2]

Abstract The aim of this study is the complete physicochemical characterization and strain rate effect multi-scale analysis of a new fully recycled carbon fiber reinforced composites for automotive crash application. Two composites made of 20% wt short recycled carbon fibers (CF) are obtained by injection molding. The morphology and the degree of dispersion of CF in the matrixes were examined using a new ultrasonic method and SEM. High strain tensile behavior up to 100 s-1 is investigated. In order to avoid perturbation due to inertial effect and wave propagation, the specimen geometry was optimized. The elastic properties appear to be insensitive to the strain rate. However, a high strain rate effect on the local visco-plasticity of the matrix and fiber/matrix interface visco-damageable behavior is emphasized. The predominant damage mechanisms evolve from generalized matrix local ductility at low strain rate regime to fiber/matrix interface debonding and fibers pull-out at high strain rate regime.

✉ H. Meftah
mefteh.hassen988@gmail.com

S. Tamboura
sahbi.tamboura@gmail.com

J. Fitoussi
joseph.fitoussi@gmail.com

H. BenDaly
hachmi.bdaly@gmail.com

A. Tcharkhtchi
abbas.tcharkhtchi@ensam.eu

[1] LMS, ENISo, Université de Sousse, BP264 Cité Erriadh, 4023 Sousse, Tunisie

[2] Laboratoire PIMM, UMR 8006 CNRS, Arts et Métiers ParisTech, 75013 Paris, France

Keywords Recycled composite · Carbon fibers · High strain rate · Fiber/matrix bond · Fiber pull out

1 Introduction

Over the last three decades, the use of short fiber reinforced polymer composites in automotive applications has seen an exponential increase. Such composites provide upgraded mechanical properties, enhanced crashworthiness and efficient lightweight solution. As the worldwide volume of composite usage grows, in fact in Europe approximately 1 million tons of composites are manufactured each year [1], the waste coming from manufacturing processes or end-of-life products considerably increases. From the environmental and economic viewpoint, this has raised an awareness of the need to recycle them and turning them into a valuable resource.

Due to their complex composition (fibers, matrix and fillers), composites are naturally difficult to recycle entirely. That is the reason why in many cases, only fibers can be recovered during recycling process. Several methods to remove the resin and recover virgin-like fibers from composites waste have been developed [2, 3]. Among them, because of its efficiency, the pyrolysis process is the most widespread used technic. The latter consists in heating the composite to recycle up to 450 °C to 700 °C in the nearly absence of oxygen to volatilize the matrix [2] and then recover the remaining fibers.

From cost and mechanical properties point of view, carbon fibers after recycling are a very interesting. In fact, after pyrolysis glass fibers, which represent more than 90% of the composites reinforcement worldwide, are highly degraded. Comparatively, their mechanical properties drop by 70% while carbon fibers properties decrease does not exceed 10% [4, 5]. Moreover, recycled carbon fibers cost represents only half of the virgin ones price. Furthermore, the energy needed to produce pristine carbon fibers is very high, around 286 MJ/kg [6–8] while only 5 to 10% of this energy is required to produce recycled fibers [9].

Actually, because of their high stiffness or strength to density ratio, these materials have a growing interest in transport industry. Indeed, they should be reused in new engineering materials especially for lightweight components in order to reduce vehicle weight [10, 11]. For these advantages, the worldwide demand on recycled carbon fibers keeps increasing year after year in aeronautic and automotive applications.

In automotive industry, short fiber reinforced composites are often used for crashworthiness improvement. However, their mechanical response is very sensible to strain rate loading [12]. Especially for thermoplastic composites, specific local strain rate effect can be observed [13]. Thus, a multi-scale analysis involving microstructure and damage analysis is often needed to understand the strain rate effect in short fiber reinforced composites.

The current work is divided in two parts: in one hand, two recycled carbon fiber reinforced composites obtained by injection are elaborated and characterized. The first composite uses a 100% recycled Polypropylene/Polyethylene blend matrix (RPP) while the second one is made of an equivalent polypropylene. On the other hand, we propose an optimized experimental testing procedure able to characterize the mechanical behavior of theses composites subjected to rapid loading. The experimental methodology is built upon monotonic high-speed tensile tests performed at different crosshead velocities. The main difficulty was to obtain uniform stress/strain distribution and constant strain rate [13]. Indeed, specific inertia effects encountered during high-speed tensile tests make difficult the achievement of reliable measurements

and repeatability. In this paper, a numerical optimization of the specimen geometry using ABAQUS finite element code has been performed in order to reduce waves perturbations and to obtain homogeneous strain distribution and constant strain rate in the specimen's effective zone. The explored strain rate range is from $\dot{\varepsilon} = 10^{-3}\ s^{-1}$ (quasi-static) to 100 s^{-1}. Finally, macroscopic results are correlated with a fractography investigation using Scanning Electronic Microscope.

2 Materials and Experimental Methods

2.1 Constitutive Materials of the Elaborated Composites

In this study two kinds of recycled composites were elaborated using recycled carbon fibers (CF) with an average length of about 180 μm. Two types of matrixes were used: a recycled polypropylene / polyethylene blend (RPP) and an equivalent virgin polypropylene (PP). The recycled carbon fibers were obtained by pyrolysis and then milled to produce fibers with a density of 1.8 g/cm^{-3}, a diameter of 7 μm and a nominal length of 180 μm. These CF have a Young's modulus and tensile strength of 230 GPa and 3.5 GPa respectively as indicated in the data sheets provided by the manufacturer. On the other hand, the recycled matrix was obtained by confidential chemical process.

2.2 Composites Elaboration

Prior to compounding, the two matrixes were dried in an oven to remove residual moisture. RPP in granular form (respectively PP) and 20% weight content of recycled carbon fibers were mixed using a twin screw extruder Haake Termo. The carbon fiber/ matrix mixture was fed by a metering device at a rate of 600–700 g/h to move into the extruder through a hopper. The screw configuration was selected so as to minimize mechanical damage of the fibers. The extruder was operating at a total throughput of 700 g/h with a screw speed of 150 rpm and a die temperature of 210 °C. Once the granules compounds were obtained they were dried in an oven before being molded using a DK CODIM 175/410 injection molding press with a clamping force of 1750 kN. The injection temperature was set at 230 °C with an injection speed of 15 mm/s. The injection mold was maintained at 50 °C in order to allow the crystallization of the matrixes. Finally after a total after cooling time of 6 s, plates of 125x125x2.5 mm dimensions were obtained.

2.3 Physicochemical Characterization

Thermal analysis provides several characterization techniques of polymers with regards to their impact resistance properties. In this study, differential scanning calorimetry (DSC) and Dynamic Mechanical Analysis (DMA) [14] were used.

2.3.1 Differential Scanning Calorimetry (DSC)

Crystallization behavior and melting characteristics of the two matrixes were characterized with the help of a DSC TA Q1000 thermal analyzer. The samples were sealed in an aluminum pan and then heated from 10 °C with a subsequent heating of 10 °C per minute up to 180 °C and hold for 5 min in

order to erase the mechanical and thermal history. Afterwards, the crystallization in the two matrixes and composites as well was investigated by cooling the pans from 180 °C to 10 °C at a cooling rate of 10 °C per minute. During a second heating run, with the same heating rate, from 10 °C to 180 °C, the melting point and the enthalpy of fusion of each sample were determined.

2.3.2 Dynamic Mechanical Analysis (DMA)

Due to the limitation of detecting the glass transitions corresponding to the different polymers in the blends [15–17], dynamic mechanical tests were carried out on samples with a dynamic mechanical analyzer (TA DMA Q800) comprising a temperature programmer and a controller. The experiment was conducted in a 3 points bending from −140 to 100 °C at a frequency of 1 Hz with a programmed heating rate of 2 °C min^{-1}. In order to settle sub-ambient temperature, liquid nitrogen was used.

2.4 Microstructure Analysis

In order to characterize the microstructure of a short fiber reinforced composite, qualitative and quantitative analysis is performed using a non-destructive ultrasonic technique. In this study, an original method dedicated to fiber orientation analysis is proposed. Two probes were immersed into a water tank, one transmitting the ultrasonic wave (E) and one receiving it (R). They were separated by a known and constant distance (d) during the entire measurement procedure. As a preliminary step, the wave propagation velocity in water, V_0, is measured using an oscilloscope in order to determine the crossing time between the two probes (distance/time). In a second step, the composite sample is placed perpendicularly between the two probes as shown in Fig. 1. Thus, longitudinal waves are generated and propagate through the specimen width. If assuming that all the fibers are contained in the plane of the plate, one can consider that the longitudinal wave velocity V_L depends only on the fiber content. Indeed, in that case, the wave velocity does not depend on the fiber orientation distribution.

Subsequently, the sample is rotated by an angle i (angle of incidence) in order to give rise to transversal waves (T) which propagates through the specimen in a direction (r) defined by the Snell's law:

$$\frac{\sin(i)}{V_0} = \frac{\sin(r)}{V_T}$$

Where V_T is the velocity of transversal waves in the sample.

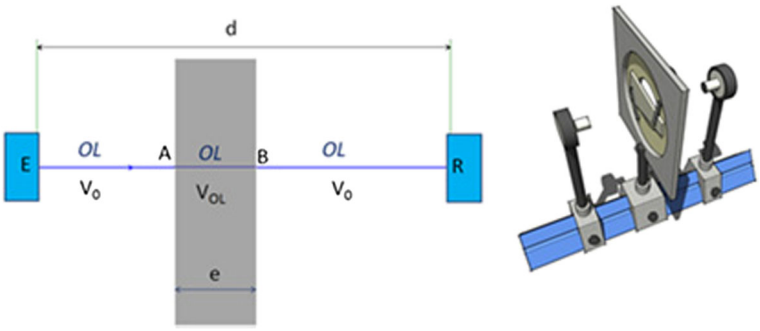

Fig. 1 Schematic representation of the ultrasonic device

During propagation of transversal waves, the sample is submitted to shear (Fig. 2) in the plane ($\vec{i}$, $\vec{n}$). Rotating the sample around the normal axis ($\vec{n}$), generate a variation of V_T directly related to the relative orientation of the fibers. In fact, if the fibers are oriented in the shear plane (Fig. 2 a), they offer a high section to shear. Therefore, higher values of V_T are measured. On the other hand, when the fibers are oriented perpendicularly (Fig. 2 b), the sheared section and the wave velocity are at their lower values. Consequently, the evolution of V_T versus the rotation angle around the normal will indicates clearly the predominant fiber orientation. Moreover, one can define an indicator k (%), the acoustical birefringence coefficient, related to the fiber orientation intensity as:

$$K = \frac{V_{OTmax} - V_{OTmin}}{V_{OT\ av}}$$

Where $V_{OT\ av}$ is the average value of V_{OT}.

According to Fig. 1, the velocity of the longitudinal wave in the material is given by:

$$V_L = \frac{e}{t_e - \frac{d-e}{V_0}} \tag{1}$$

Where t_e is the crossing time between the two probes given by:

$$t_e = \frac{EA + BR}{V_0} + \frac{AB}{V_T} \tag{2}$$

Finally, the velocity of the shear wave in the material is given by eq. 3:

$$V_T = \frac{eV_0}{\sqrt{e^2 + 2eV_0(t_e - t_0)\cos i + V_0^2(t_e - t_0)^2}} \tag{3}$$

2.5 High-Speed Tensile Characterization

2.5.1 High-Speed Tensile Device

In the current study, High-speed tensile tests have been realized at different strain rates using a servo-hydraulic test machine (Schenck) which can reach a crosshead speed ranging from

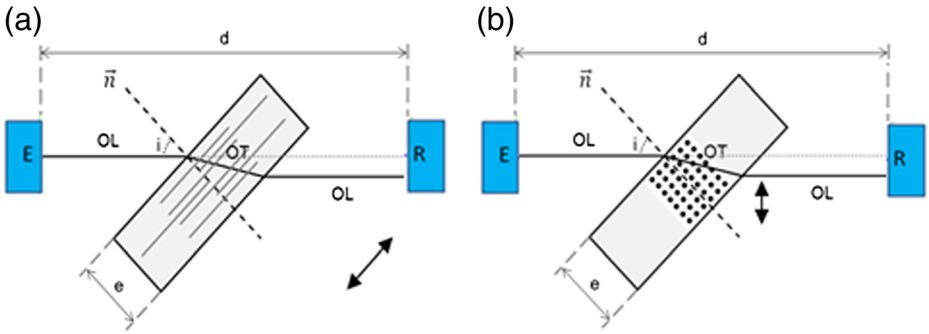

Fig. 2 Methodology of determination of the fiber orientation (a) longitudinal fibers (b) perpendicular fibers

10^{-3} m/s to 20 m/s. Furthermore, the applied force is measured by a piezoelectric crystal load cell of a 50 kN capacity. Composite specimens were gripped between the load cell (upper extremity) and the moving device (lower extremity) and tensile loading was performed until total failure.

A sliding bar is accelerated over a straight displacement of 135 mm before its contact with the hydraulic jack in order to reach the nominal crosshead velocity before the load beginning. Once the contact takes place, the specimen is then subjected to tension at a constant displacement rate. In order to attenuate partially the perturbation due to mechanical waves caused by the dynamic shock, the material and the geometry of a damping joint, placed between the sliding bar and the hydraulic jack, have been optimized [18].

In order to measure the local deformation in the specimen, a contactless technique is adopted using a high speed camera (FASTCAM-APX RS) with a capacity of 250,000 frames per second to record pictures during high speed tensile test [19].

2.5.2 Specimen Geometry Optimization

High-strain rate testing is a difficult and a complex field. Indeed, dynamic mechanical behavior characterization of composites causes some experimental difficulties [18, 20]. As matter of fact, during high speed testing, non-uniform loading and inertia effects raise some challenges. Therefore, a solid experimental methodology is needed to ensure measurement repeatability. In this study we aimed to optimize numerically the geometry of the specimen using ABAQUS finite element (FE) code [21] in order to be able to get a uniform strain distribution and a constant strain rate in the specimen representative zone [19, 21–23]. To this aim, perturbations due to inertial effect and wave propagation should be reduced.

Consequently, the aim of the optimization methodology described hereafter was to reach rapidly a stabilized strain distribution and a constant strain rate within the specimen gauge section at the beginning of the loading. The optimization of the specimen geometry is then carried out in 4 steps [18]:

- First, a dynamic tensile test is performed in order to measure the displacement induced at the specimen extremities. At the beginning of the tensile test, the shock effect is limited by a damping joint until its full compression. Consequently, the specimen is submitted to a progressive acceleration resulting from the deformation of the damping joint until total compression. After the rising time, (t_r), for which the damping joint is fully compressed, the induced displacement rate between the specimen extremities becomes constant. Several damping joint materials have been tested in order to reduce the rise time. The optimal rise time (t_r) using a Nitrile joint is estimated experimentally and ranges between 10^{-4} and 10^{-5} s as a function of the nominal test velocity and the adopted joint thickness.
- Once the rise time evaluated, boundary conditions are numerically applied on the specimen extremities in terms of imposed velocity in order to compute the dynamic response of the latter, Fig. 4(b).s
- Assuming that the specimen behaves as an elastic anisotropic solid, an iterative optimization process is performed using finite elements simulations for the sake of the optimal geometrical parameters L_1, L_2, L_3, L_4 and R as sketched in Fig. 3(c) which ensure stress

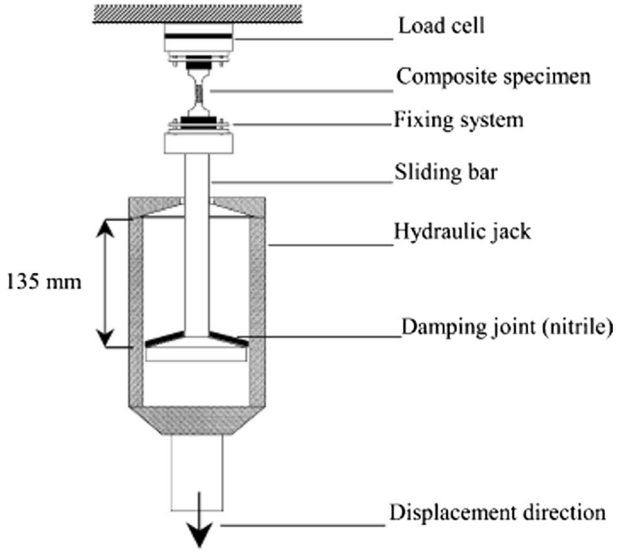

Fig. 3 Schematic high-speed tensile tests servo-hydraulic device

wave effects diminution and generate homogeneous stress/strain fields and constant strain rate at the effective zone of the specimen.

- Finally, in order to validate the optimized geometry, high-speed tensile tests are performed on the composite specimen and compared to simulation results (Fig. 4 (a)). The geometry of the optimized dumbbell-shaped specimen is summarized in Table 1.

Figure 4 (c) shows the predicted longitudinal tension stress distribution for the optimized specimen submitted to an imposed velocity of 4 m/s which corresponds to a theoretical value of strain rate of $\dot{\varepsilon} = 400\ s^{-1}$. Moreover, it is clearly notable that, although some very localized stress concentration, stress field in the center of the composite specimen is homogeneous. However, it should be noted that because of a progressive micro-displacement in the gripping system, the strain rate value measured in the specimen gauge length can be 20% to 30% lower than the theoretical one ($400\ s^{-1}$).

The spatio-temporal profile of the longitudinal stress ($\sigma 11$) calculated along the central line of the composite specimen is represented in Fig. 5. Based on this latter, one can notice that the choc wave vanishes very quickly. In fact, after only $3.5\ 10^{-5}$ s the stress distribution becomes relatively homogeneous for an average stress of 1.2 MPa.

3 Results and Discussion

3.1 Material Characterization

3.1.1 Carbon Fiber

Figure 6 shows scanning electron micrographs of the carbon fiber's morphology and geometry. The recovered fibers have an average length around 200 μm and diameter of 7 μm as

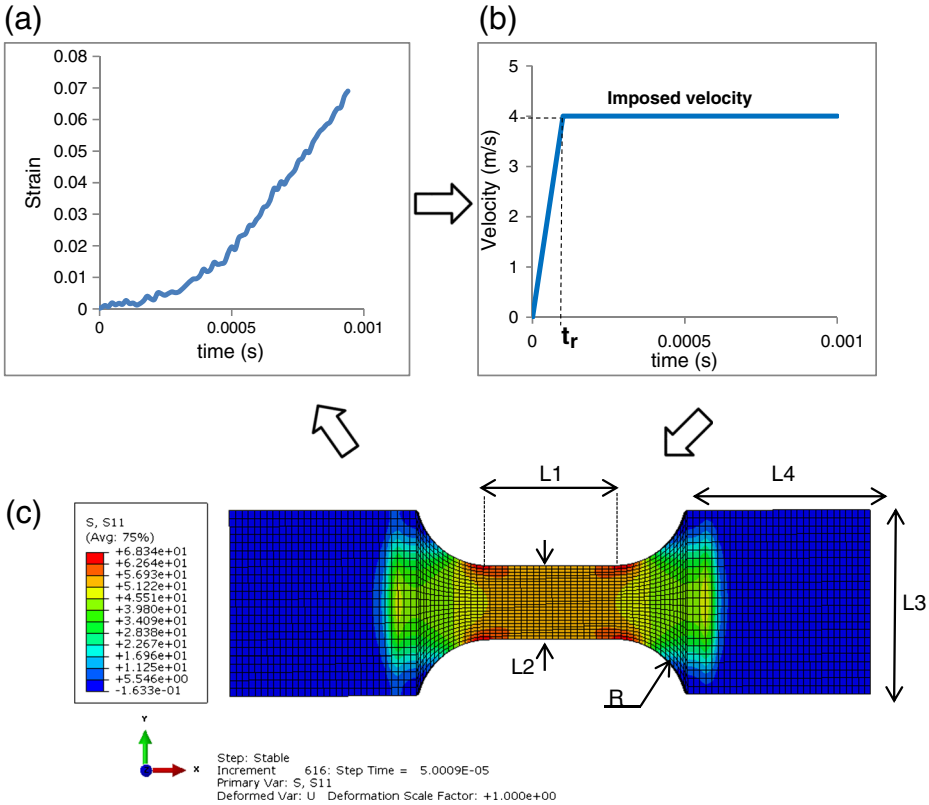

Fig. 4 **a** Experimental and simulation data **b** Boundary condition (c) Longitudinal tension stress (σ11) distribution calculated for the optimized dumbbell-shaped specimen submitted to a tensile test (V = 4 m/s rise time = 2 10^{-4} s)

mentioned in their datasheet. In addition, Fig. 5 (C and D) show that the fibers have a radial microstructure and a noticeably rough surface which is due to the absence of sizing agents.

3.1.2 Physicochemical Properties of the Different Materials

The melting and crystallization phenomena of the matrixes and composites were studied by measuring the equilibrium melting temperature (T_m), the crystallization temperature (T_c).

The crystallinity (Xc) was calculated using the following equation:

$$X_c = \frac{\Delta H_m x\ (mc/mp)}{\Delta H_0}\ \text{x}\ 100$$

Table 1 Optimized composite specimen dimensions for high speed tensile test

	L1 (mm)	L2 (mm)	L3 (mm)	L4 (mm)	R (mm)
Optimized specimen	10	6	15	15	6

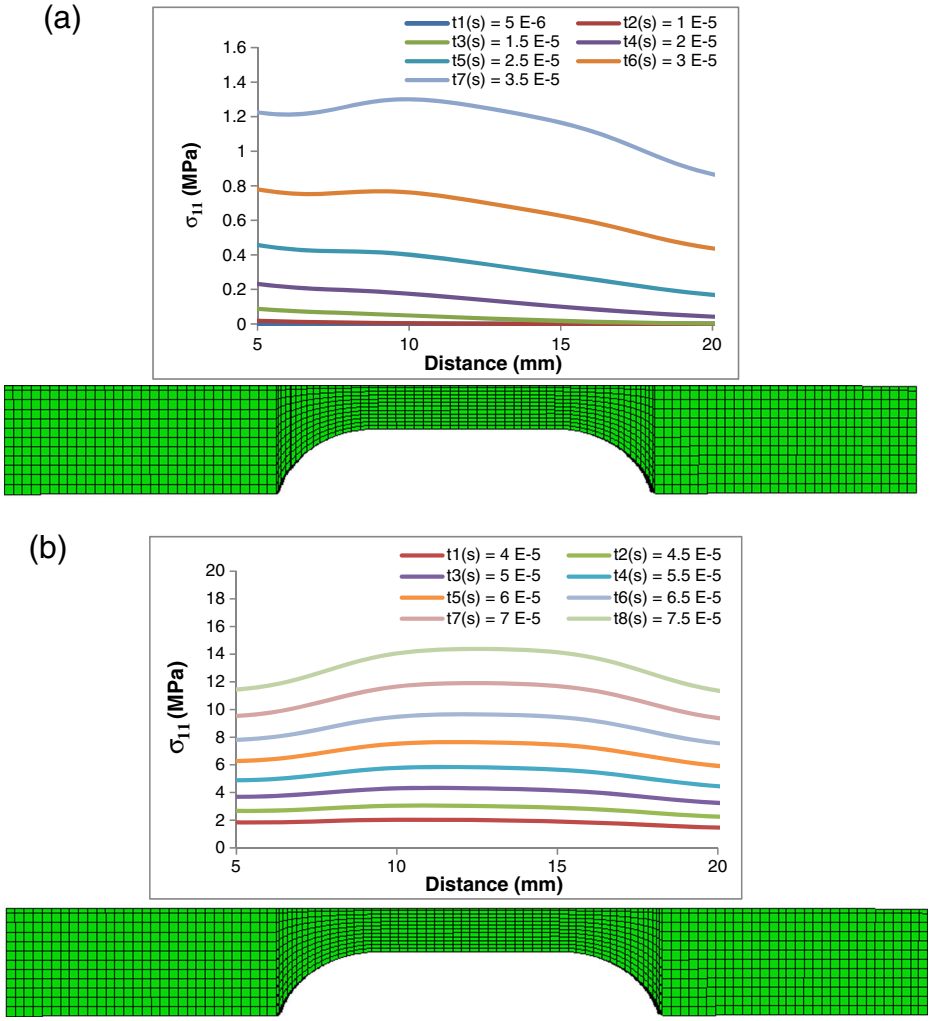

Fig. 5 Spatio-temporal profile of the longitudinal stress calculated along the central line of the specimen. Loading conditions: imposed velocity V = 4 m/s. (**a**) First steps and (**b**) next steps

Where ΔH_m is the melting enthalpy, $\Delta H_0$is the theoretical enthalpy of PP and PE at 100% crystallinity ($\Delta H_0 = 207$ j.g^{-1} for the PP and 293 j.g^{-1} for the PE [Roger L. Blaine]), mc the mass of the PP or PE in the sample and mp is the total mass of the sample.

The DSC thermograms are shown in Fig. 7. It is clearly evident from the curves that the PP represents a single main endothermic peak related to the melting, at 167 °C and one exothermic peak corresponding to the crystallization at 133.5 °C while the blend represents two melting peaks one at 128 °C and a second at 164.5 °C and two cold crystallization peak as well at 117 °C and 125 °C. The results represented in Table 2 show in one hand that with the addition of PE to PP, the crystallinity of this later in the blend remains the same. In the other hand, it can be deduced that the melting and crystallinity temperatures for matrixes and theirs composites are substantially the same however the crystallinity increases by 7 to 8%.

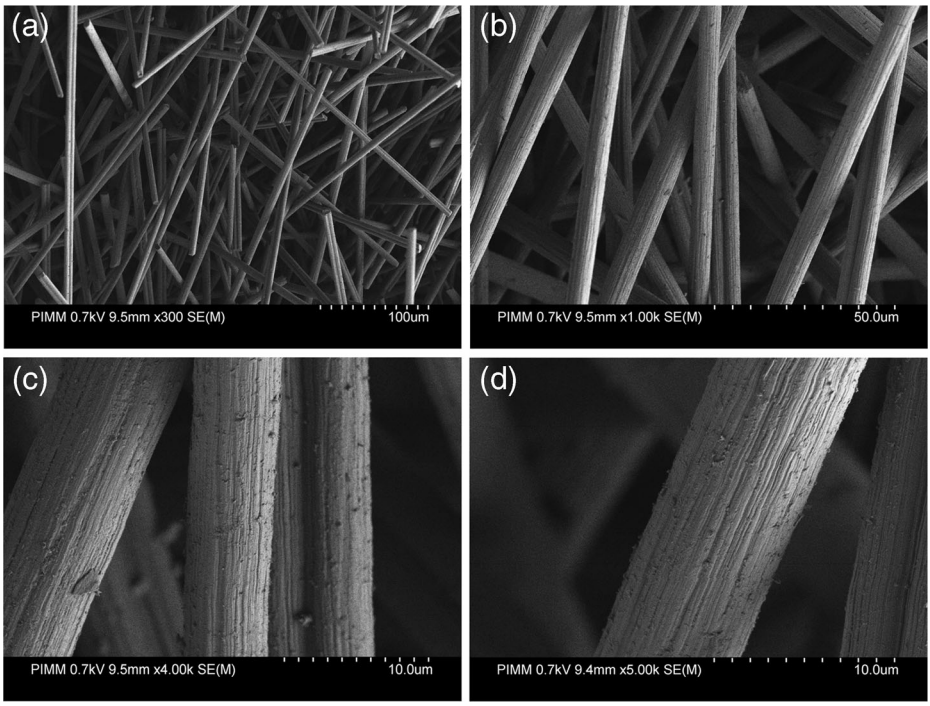

Fig. 6 SEM images of recycled CF

Beyond its exceptional applicability in the measurement of glass transition temperature (T_g), storage modulus (E') and loss modulus (E") of polymers, dynamic mechanical analysis is a strong tool in studying of miscibility, internal friction which can be related to damping behavior, phase morphology of polymer blends and molecular mechanism of any type of transitions occurred in polymers [24, 25]. The dynamic mechanical properties of the recycled blend and the pure polypropylene illustrated in Fig. 8 represent the plots of the storage (E'), viscous (loss E") modulus and damping (tan δ) of the two matrixes. These curves show different transition temperatures recapitulated in Table 3. It is clearly noticed that there is a presence of two relaxation motions assigned as αc (T_1 = 46 °C), and α (T_2 = −2 °C) in the order of decreasing temperature: the αc-motion and the α-motion are attributed to the relaxation of crystals and to the glass transition temperature of PP ($T_{g\text{-}PP}$) respectively. T_4

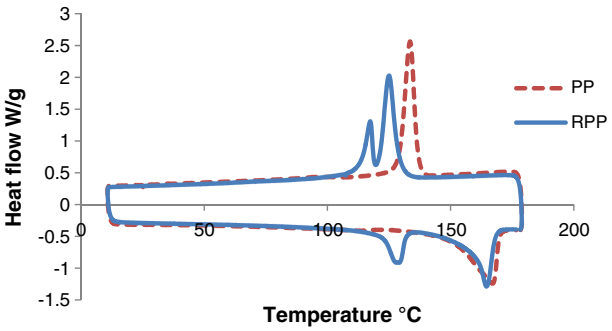

Fig. 7 DSC thermogram of RPP blend and pure PP

Table 2 Melting and crystallinity behavior of the matrixes and composites

Sample		Crystallization		Melting behavior		Xc (%)
		T_c (°C)	ΔH (J g^{-1})	T_m (°C)	ΔH (J g^{-1})	
RPP	PE	117	154.58	126.8	175.91	65.72
	PP	125	66.91	163.3	65.56	31.67
PP		133	65.46	167.3	66.20	31.98
RPP-CF180	PE	117	145.83	127.65	217.39	74.19
	PP	125	68	164.15	79.96	38.63
PP-CF180		134.68	65.81	166.63	80.26	38.77

(−125 °C) corresponds to the glass transition temperature of polyethylene [26, 27]. As for the transition temperature at −47 °C, it is related to the β-transition of polypropylene.

The results show also that α-transition of PP and PE in the blend is nearly the same as pure polymers, indicating that α-transition of PP and PE in the blend is nearly the same as pure polymers, indicating that RPP is an immiscible polymer blend [27].

3.2 Morphological Properties of the Injected Parts

The orientation distribution of the fibers in the matrix has been investigated by ultrasonic analysis performed at different points of the composite plate as shown in Fig. 9.

Figure 10 shows an example of obtained results for RPP-CF180 sample. In the left curve, the peaks at 90° and 270° correspond to the predominant fiber orientation. The orientation intensity is characterized by K. After ultrasonic measurement in 9 locations of the plate, one can note that the composite plate represents two slightly different microstructures where the fibers are well oriented in the mold flow direction but with a different k coefficient. In fact, in the left and right zones the average of value of k is about 31% but significantly decreases in the middle of the plate with an average value around 14%. The latter shows a spatial non-homogeneity of fibers orientation distribution throughout the plate.

To complete these results, SEM investigation of the microstructure of the composites was carried on polished longitudinal section of a specimen. The micrograph (Fig. 11) confirms that the recycled carbon fibers are evenly distributed in the matrix and are mainly aligned along the injection direction with a mean length of 100 μm. In fact one can clearly notice that the composite microstructure is divided in three zones: two shell zones of 1 mm thickness where the fibers are mainly oriented in the mold flow direction and a 0.5 mm core zone where the orientation of the fibers is perpendicular to the direction of injection.

3.3 Dynamic Behavior of the Injected Parts

3.3.1 Optimization Validation

A comparison between experimental and numerical rapid tensile test at an imposed velocity of 4 m/s is shown in Fig. 12. A good correlation is observed. After a measured a rise time of about 5×10^{-5} s the strain rate becomes stable and beyond this latter the specimen is submitted to a homogeneous stress of about 4 MPa which corresponds to the elastic behavior first stages [19, 28]. Thus, on can affirm that the measurement of the Young's modulus is accurate. For a 4 m/s tensile test, the theoretical value of $d\varepsilon/dt$ should be of 400 s^{-1} after stabilization; however

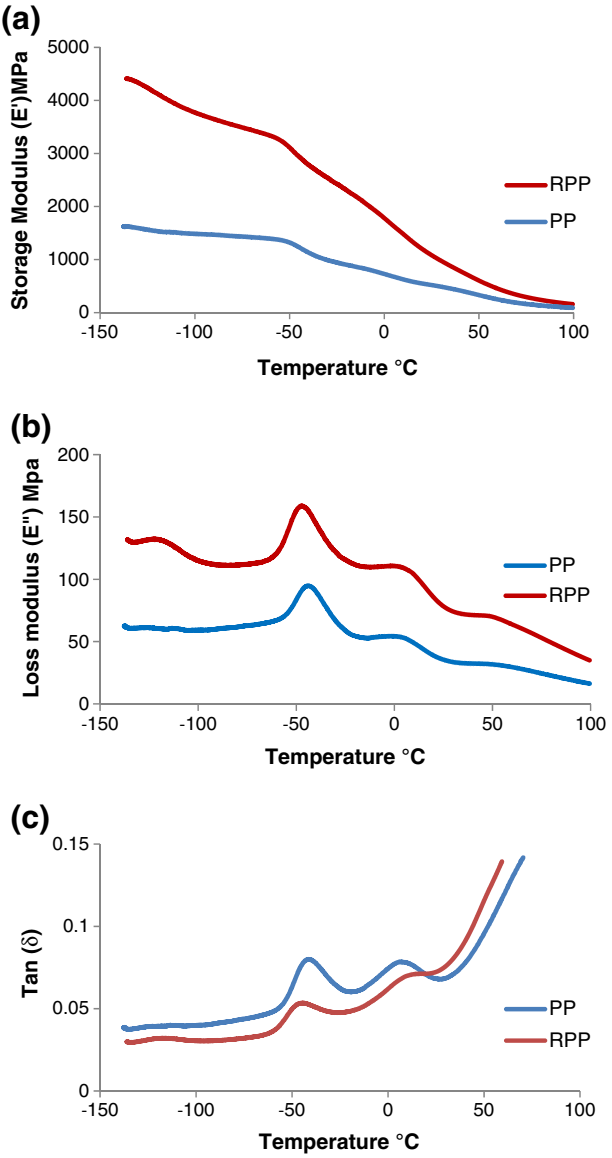

Fig. 8 Storage modulus E', loss modulus E" and damping (tan δ) spectra of the two matrixes

it is not the case. In fact, experimental strain rate is about 300 s^{-1}, which means 25% lower than the theoretical one.

On the basis of the very good agreement between numerical results shown in Fig. 12 and the accurate obtained experimental curves, one can claim that our optimization procedure validates the proposed geometry.

Figure 13 shows examples of strain evolution for different strain rate measured in the central zone of the specimen. These measurements are obtained using a high speed camera (FASTCAM-APX RS) allowing to follow the relative displacement of two circular marks pre-

Table 3 Different transition temperatures of PP and RPP, obtained from E" and tan δ spectrum

	T_1 (°C)	T_2 (°C)	T_3 (°C)	T_4 (°C)
PP	46	−2	−48	-
RPP	45	−2.5	−47	−125

drawn on the specimen surface. Therefore, strain evolution can be determined using image analysis. After a damping stage, characterized by a progressive increase of strain rate, the strain rate becomes constant. Thus, strain rate is easily determined from the slope of the linear part.

3.3.2 Strain Rate Effect on the Overall Tensile Response

Figure 14 represents the different stress-strain curves of the matrixes and their composites over a range of strain rates varying from 7.10^{-3} to 100 s^{-1} at room temperature of 293 K. For both quasi static and high speed loading, one can notice that experimental results exhibit the features of large deformation material response. Indeed, four stages are present: initial elasticity, subsequent yield followed by strain softening and strain hardening.

Table 2 represented above shows that the melting and crystallization temperatures are similar for both unreinforced and reinforced RPP and PP matrixes. Thus, it can be stated that the thermo-mechanical behavior of the thermoplastic matrixes is not significantly affected by the presence of the carbon fibers. However, the mechanical behavior of the matrixes is affected by strain rate independently of possible visco-damage effects [23].

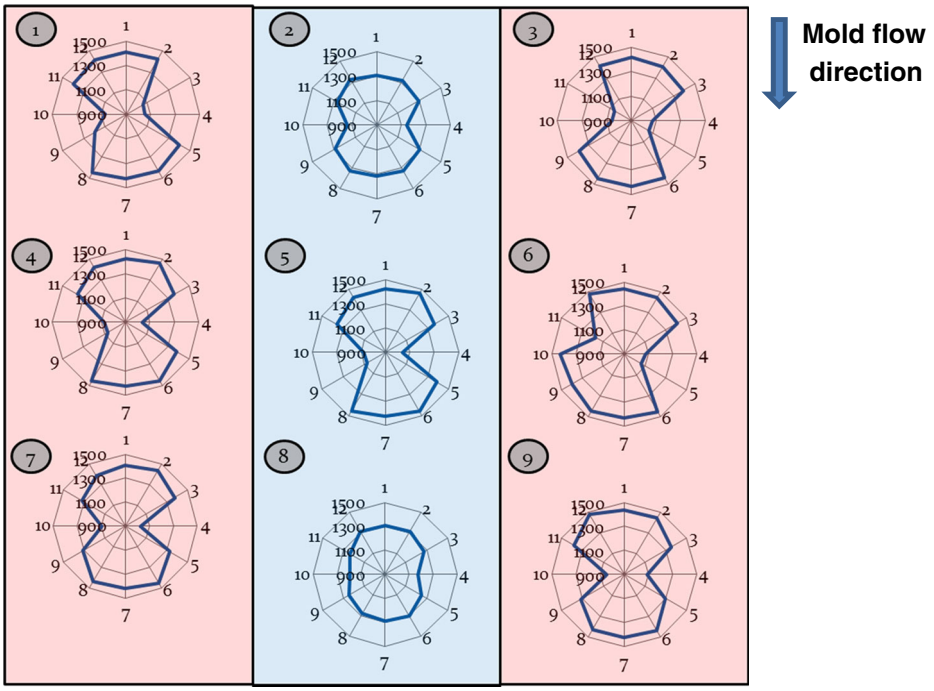

Fig. 9 Ultrasonic point's measurement in the composite plate

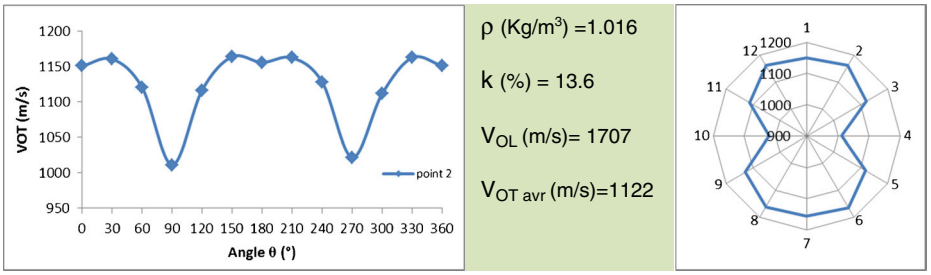

Fig. 10 Example of obtained curves with fiber direction for RPP-CF180 in point 2

The obtained tensile curves show clearly that the overall behavior is highly strain rate sensitive: the global stress level increases with the increase of strain rate. However, no significant variation of the initial slopes of the stress-strain curves is observed for each material. Thus, one can affirm that the elastic modulus remains insensitive to strain rate.

It is easily noticeable that the RPP shows better mechanical properties than the virgin PP. In fact, at quasi-static strain rate yield strength and plastic deformation of RPP are respectively of 24 and 21 MPa and an impressive strain at rupture that can reach 500% is observed. Whereas PP is characterized by yield strength (YS) of 20 MPa and a plastic deformation value of 18 MPa and a failure strain that does not exceed 300%. Therefore, the corresponding carbon fibers reinforced composites inherit the same tendency. Indeed, Fig. 14 shows that RPP-CF180 presents betters mechanical performances than the PP-CF180.

With the increase of strain rate, the mechanical properties of the different thermoplastic matrixes and composites are affected. The evolutions of the main mechanical characteristics are represented in Fig. 14 versus strain rates.

Figure 15 (a) affirms as mentioned above that the different materials elastic moduli are insensitive to strain rate loading. On can notice that, even if the pure matrixes moduli are of the same order of magnitude, the corresponding composites moduli are very different. Indeed, the lower value obtained for the non-recycled matrix composite emphasize a bad fiber-matrix interface which does not assure load transfer.

Otherwise yield stress (YS), ultimate tensile strength (UTS) and failure strain (Er) are dramatically affected when increasing strain rate as show in Fig. 15 (b), (c) and (d): both UTS

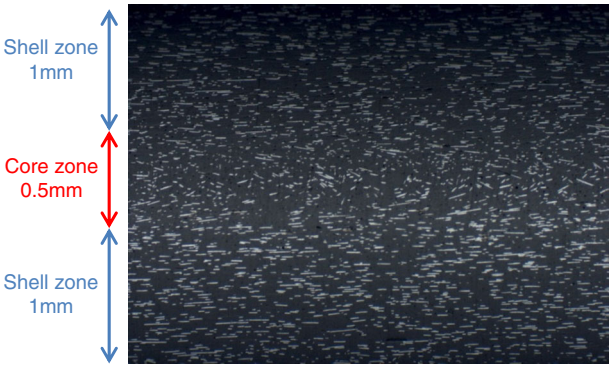

Fig. 11 Microscopic observation of the composite PPr-CF180 structure

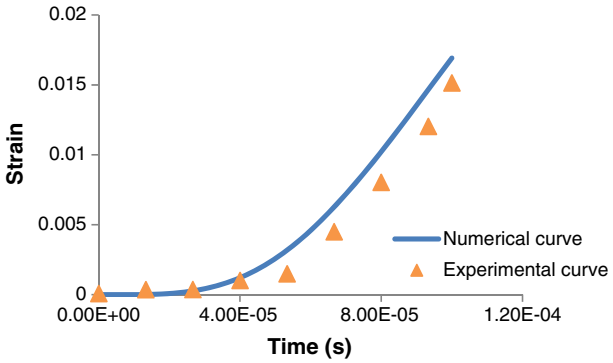

Fig. 12 Evolution of the strain in the central zone of the specimen. Comparison between experimental and numerical results obtained for the composite optimized geometry

and YS increase progressively for a strain rate lower than 10 s^{-1} and at a rapid rate for the dynamic strain-rate regime. As for Er, it shows a remarkable drop before stabilizing and becoming almost constant for high speed loading.

3.3.3 Local Damage and Local Deformation Mechanisms Analysis

In order to emphasize the local damage and deformation mechanisms, qualify the matrix-fiber interface and determine the effect of strain rate on the latter, SEM investigation were realized on the tensile failed specimens for quasi-static and dynamic tensile loding. The SEM micrographs of the RPP-CF180 specimens tested under different strain rate tensile loading are shown in Fig. 15.

It is noticeable that, at low strain rate (0.1 s^{-1}), a good fiber-matrix adherence allows high local plasticity of the matrix. As shown in Fig. 16 (a), fiber-matrix interface debonding finally appears after a very marqued ductility of the matrix.

With the increase of strain rate, one can observe (Fig. 16 (b)-1 s^{-1}) a significant decrease of the local ductility of the matrix. At 10s^{-1} (Fig. 16 (c)), Local deformation are concentrated around the fibers. On can speak about an interphase zone plasticity leading to a cavity growing

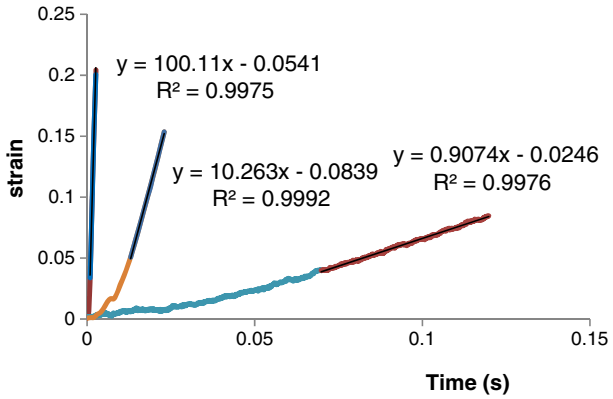

Fig. 13 Typical contactless strain measurements at various high strain rates for RPP-CF180

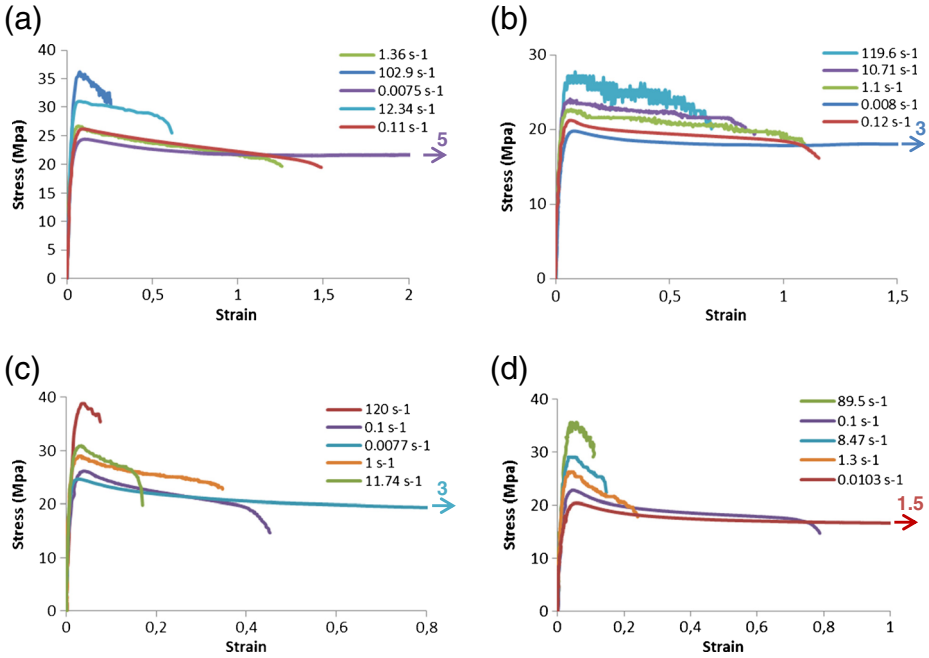

Fig. 14 Experimental high strain rate tensile curves. (**a**) RPP (**b**) PP (**c**) RPP-CF180 (**d**) PP-CF180

around the fibers. Far from this zone, matrix seems to be fragile. Finally, at 100 s^{-1} (Fig. 16 (d)), no matrix ductility is observed even in the interphase zone. Fiber pull-out and fibers breakage lead rapidly to subsequent failure.

This fractography analysis shows clearly that damage depends on the fiber-matrix interface strength and strain rate loading. Moreover, local damage is highly dependent on the matrix local plastic deformation strain rate sensitivity. Final failure strain rate dependence emphasized in Fig. 15 (e) is easily justified by the coupled effect of the local viscoplasticity of the matrix and the fiber-matrix visco-damage.

On the other hand, SEM fractography observation performed on PP composite specimens submitted to the same strain rates confirms the low fiber interface strength which has been also emphasized by the low Young's modulus (Fig. 15 (a)). Indeed, even for the lower strain rate for which the matrix is ductile, the whole surface of the interface is debonded without residual matrix remained bonded as it can be observed at the same strain rate for the RPP composite. On the other hand, brittle interface debonding and very limited ductility are observed from 1 s-1. Moreover, for higher strain rate, local plasticity and cavity growth take place around the fibers as described in Fig. 17.

4 Conclusion

In this work, a new fully recycled composite and a semi-virgin one: short recycled carbon fibers reinforced recycled polypropylene/polyethylene blend and virgin polypropylene

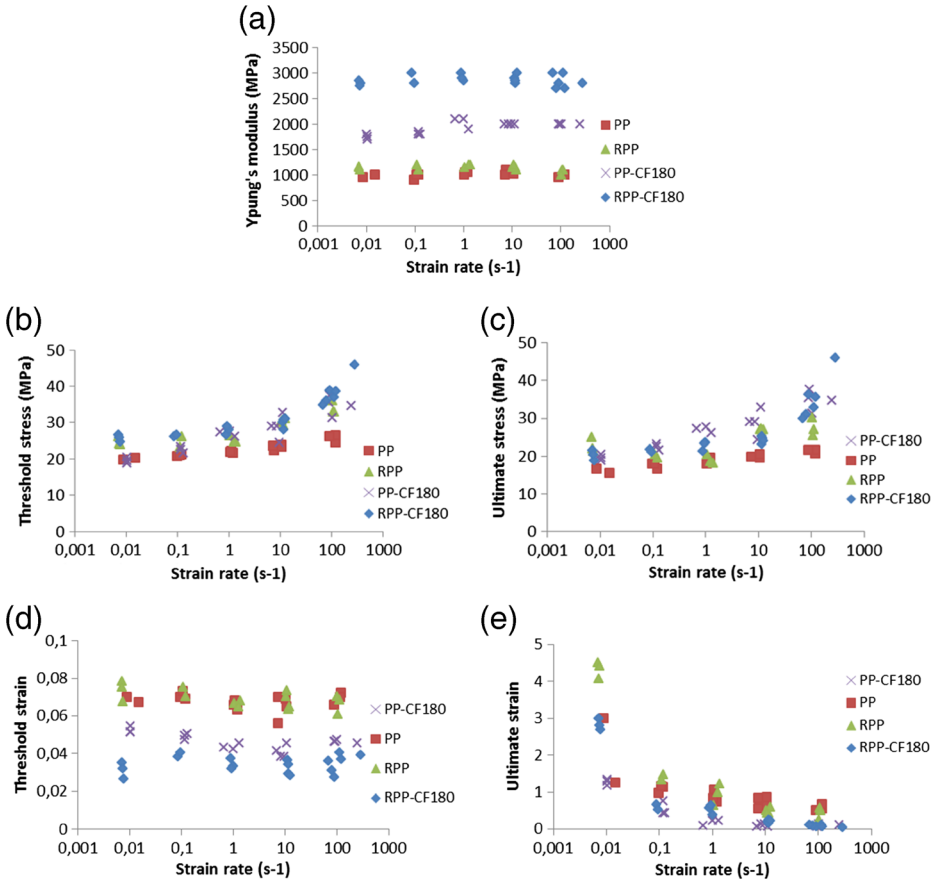

Fig. 15 Effect of strain rate: (**a**) Young's modulus, (**b**) Threshold stress, (**c**) Ultimate stress, (**d**) Threshold strain, (**e**) ultimate strain

composites for automotive applications were elaborated by extrusion and then injection molded. The composites microstructures were investigated by a new ultrasonic method and microscopic analysis showing a strong specific orientation of the fibers according to the Mold Flow Direction.

A physicochemical characterization was realized using differential scanning calorimetry and dynamic mechanical analysis in order to determine the matrixes thermo-mechanical properties and to analyze the influence of the addition of the reinforcement fibers on these latter. It has been demonstrated that the carbon fibers addition doesn't affect significantly the matrixes thermo-mechanical properties.

To study the mechanical properties of composites and matrixes under different strain rates varying from quasi-static to 100 s^{-1}, an optimization of the specimen geometry was needed. To this aim, numerical computations, using ABAQUS finite elements explicit code, were realized and the stress wave propagation that takes place during high-speed tensile tests in the specimen was analyzed. An optimum specimen geometry was chosen based on the numerical optimization and was validated experimentally. Constant strain rate and a homogeneous strain and

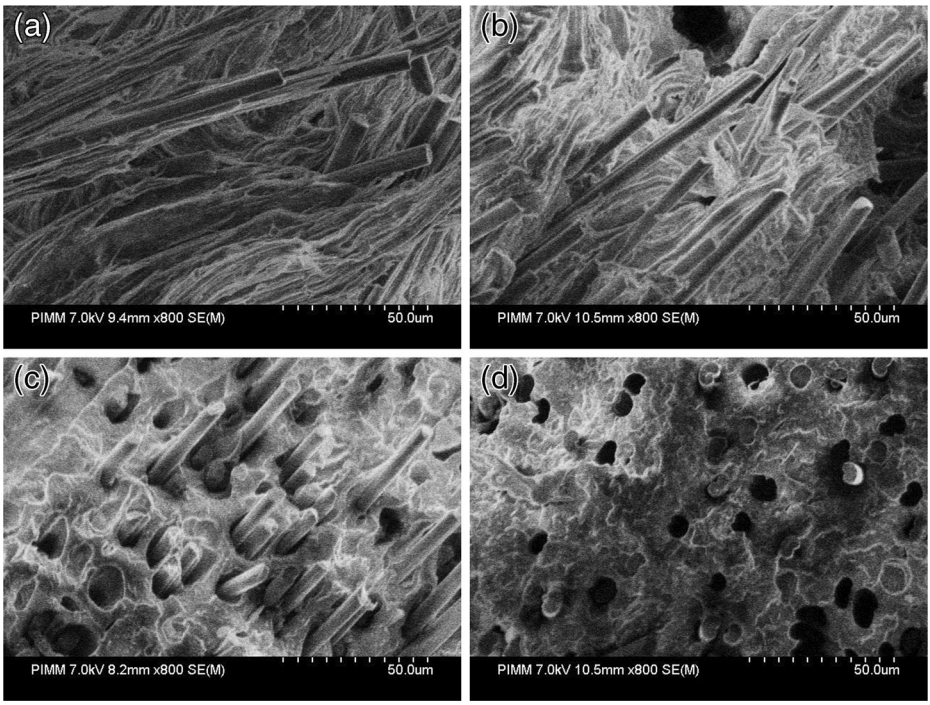

Fig. 16 Influence of strain rate on the fiber-matrix interface of RPP-CF180: (**a**) $\dot{\varepsilon}$ =0.1 s-1, (**b**) $\dot{\varepsilon}$ =1 s-1, (**c**) $\dot{\varepsilon}$ =10 s-1, (**d**) $\dot{\varepsilon}$ =100 s-1

stress in the gauge section were demonstrated by using a non-contact strain measurement and a high speed camera.

For the overall mechanic behavior, it has shown that that the introduction of recycled carbon fibers improved mechanical properties. However, lower mechanical properties of the non-recycled composite have been shown due to a lower ductility of the matrix compared to the recycled one and a bad fiber-matrix adherence.

Moreover, both RPP and PP matrixes and their corresponding carbon fibers reinforced composites are highly strain rate dependent. Indeed, mechanical characteristics, in terms of ultimate properties and damage, are very sensitive to the strain rate although the Young's modulus does not show significant variations. As the strain rate increases, noticeable effects take place: for example, when increasing the strain rate from quasi-static (0.007 s^{-1}) to120 s^{-1}, the yield strength and the ultimate tensile strength of the RPP-CF180 increase by 50% and 73% respectively and a dramatic drop of the ultimate strain by 97% is observed when the threshold strain does not seem to be significantly affected. Furthermore, SEM analysis realized on the broken tensile specimens at different strain rate highlights the influence of strain rate on the fiber/matrix interface failure highly coupled to local visco-plasticity of the matrix. Indeed, increasing strain rate leads to less ductility and more concentrated damage around the fiber-matrix interface-interphase zone.

In a further paper, all the established experimental results will be coupled with micro-mechanical and thermal aging studies and implemented into a predictive micromechanical

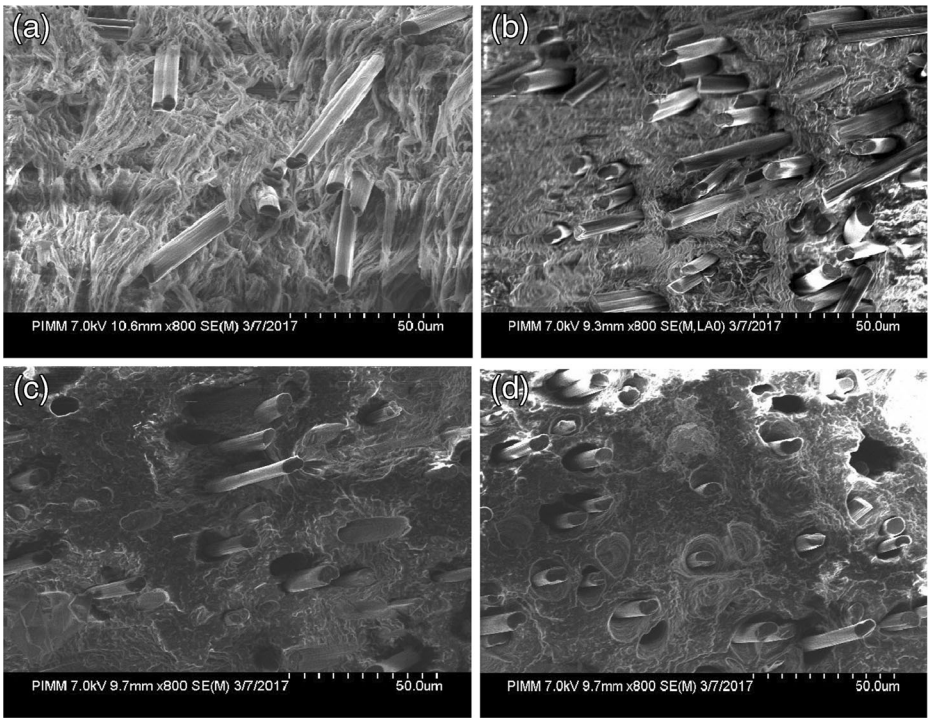

Fig. 17 Influence of strain rate on the fiber-matrix interface of PP-CF180: (a) $\dot{\varepsilon}$ =0.1 s-1, (b) $\dot{\varepsilon}$ =1 s-1, (c) $\dot{\varepsilon}$ =10 s-1, (d) $\dot{\varepsilon}$ =100 s-1

model. This multi-scale model would predict thermal aging effects on the fibers-matrix damage and on the crash properties.

References

1. Bos, G.: EU waste legislation and the composites industry. Seminar on recycling of composite materials, IFP SICOMP, Molndal, Sweden; 14th–15th May (2002)
2. Pimenta, S., Pinho, S.T.: Recycling carbon fibre reinforced polymers for structural applications: technology review and market outlook. Waste Manag. **31**(2), 378–392 (2011)
3. Pickering, S.J.: Recycling technologies for thermoset composite materials – current status. Composites Part A. **37**(8), 1206–1215 (2006)
4. Feih, S., Mouritz, A.P., Case, S.W.: Determining the mechanism controlling glass fiber strength loss during thermal recycling of waste composites. Compos A: Appl Sci Manuf. **76**, 255–261 (2015)
5. Yang, L., Sáez, E.R., Nagel, U., Thomason, J.L.: Can thermally degraded glass fiber be regenerated for closed-loop recycling of thermosetting composites? Compos A: Appl Sci Manuf. **72**, 167–174 (2015)
6. Suzuki T, Takahashi J. Prediction of energy intensity of carbon fiber reinforced plastics for mass-produced passenger cars. The Ninth Japan International SAMPE symposium, November 29–December (2005)
7. Pickering, S.J., Kelly, R., Kennerley, J.R., Rudd, C.D., Fenwick, N.J.: A fluidised–bed process for the recovery of glass fibres from scrap thermoset composite. Compos Sci Technol. **60**(4), 509–523 (2000)
8. Davidson J. Carbon fiber composites: advancements in reclamation processes and recycled material forms. Composites innovation 2007 conference proceedings. Spain: Barcelona; October 4–5, (2007)
9. Witik Robert, A., Teuscher, R., Michaud, V., Ludwig, C., Manson, J.-A.E.: Carbon fiber reinforced composite waste: an environmental assessment of recycling, energy recovery and landfilling. Compos A: Appl Sci Manuf. **49**, 89–99 (2013)

10. Pimenta S, Pinho ST, Robinson GS. Experimental study on the mechanical performance of recycled CFRP. ICCM 17, Edinburgh, July 27–31, (2009)
11. Yip HLH, Pickering SJ, Rudd CD. Characterisation of carbon fibres recycled from scrap composites using fluidised bed process. Plastics, Rubber and Composites: Macromolecular Engineering. 31,(6): University of Nottingham (2002)
12. Jendli, Z., Fitoussi, J., Meraghni, F., Baptiste, D.: Anisotropic strain rate effects on the fibre–matrix interface decohesion in sheet moulding compound composites. Compos Sci Technol. **65**(3–4), 387–393 (2005)
13. Esmaeillou, B., Fitoussi, J., Lucas, A., Tcharkhtchi, A.: Multi-scale experimental analysis of the tension-tension fatigue behavior of a short glass fiber reinforced polyamide composite. Procedia Engineering. **10**, 2117–2122 (2011)
14. Sichina, W.J.: Thermal Analysis for the Characterization of Polymer Impact Resistance. (2000)
15. Man Night, M.J., Paul, K.F.E.D.R., Newman, S.: Polymer Blends, vol. 1, p. 185. Academic Press, New York (1978)
16. Namita Rry Choudhury, Chaki T.K, BhowmIick, Anil K. Thermal characterization of thermoplastic elastomeric natural rubber-polypropylene blends. Thermochim Acta, 176 (1991) 149–161 Elsevier Science Publishers B.V., Amsterdam
17. Locke, C.E., Paul, D.R.: Chlorinated polyethylene modification of blends derived from waste plastics. Part II: Mechanism of modification Polymer Engineering & Science. **13**(4), 308–318 (1973)
18. Fitoussi, J., Meraghni, F., Jendli, Z., Hug, G., Baptiste, D.: Experimental methodology for high strain-rates tensile behavior analysis of polymer matrix composites. Compos Sci Technol. **65**(14), 2174e88 (2005)
19. Shirinbayan, M., Fitoussi, J., Meraghni, F., Surowiec, B., Bocquet, M., Tcharkhtchi, A.: High strain rate visco-damageable behavior of Advanced Sheet Molding Compound (A-SMC) under tension. Compos Part B. **82**(1), 30–41 (2015)
20. Barré, S., Chotard, T., Benzaggagh, M.L.: Comparative study of strain rate effects on mechanical properties of glass fiber reinforced thermoset matrix composites. Compos A: Appl Sci Manuf. **27**(12), 1169–1181 (1996)
21. HKS, Inc. ABAQUS theory and users manuals. V. 6.2.1; (2001)
22. Pardo, S., Baptiste, D., Décobert, F., Fitoussi, J., Joannic, R.: Tensile dynamic behaviour of a quasi-unidirectional E-glass/polyester composite. Compos Sci Technol. **62**(4), 579–584 (2002)
23. Joseph, F., Michel, B., Fodil, M.: Effect of the matrix behavior on the damage of ethylene–propylene glass fiber reinforced composite subjected to high strain rate tension. Compos Part B. **45**(1), 1181–1191 (2013)
24. Komalan, C., George, K., Kumar, P., Varughese, K., Thomas, S.: Dynamic mechanical analysis of binary and ternary polymer blends based on nylon copolymer/ EPDM rubber and EPM grafted maleic anhydride compatibilizer. Express Polym Lett. **1**(10), 641e53 (2007)
25. Dedecker, K., Groeninckx, G.: Reactive compatibilization of A/(B/C) polymer blends. Part 2. Analysis of the phase inversion region and the co-continuous phase morphology. Polymer. **39(**(21), 4993e5000 (1998)
26. Nitta, K.H., Shin, Y.W., Hashiguchi, H., Tanimoto, S., Terano, M.: Polymer. **46**, 965 (2005)
27. Nitta, K.H., Kawada, T., Yamahiro, M., Mori, H., Terano, M.: Polymer. **41**, 6765 (2000)
28. Fitoussi, J., Meraghni, F., Jendli, Z., Hug, G., Baptiste, D.: Experimental methodology for high strain-rates tensile behaviour analysis of polymer matrix composites. Compos Sci Technol. **65**(14), 2174–2188 (2005)